ARTICLES

Lipid–protein interactions in double-layered two-dimensional AQP0 crystals

Tamir Gonen[1], Yifan Cheng[1], Piotr Sliz[2,3], Yoko Hiroaki[4], Yoshinori Fujiyoshi[4], Stephen C. Harrison[2,3] & Thomas Walz[1]

Lens-specific aquaporin-0 (AQP0) functions as a specific water pore and forms the thin junctions between fibre cells. Here we describe a 1.9 Å resolution structure of junctional AQP0, determined by electron crystallography of double-layered two-dimensional crystals. Comparison of junctional and non-junctional AQP0 structures shows that junction formation depends on a conformational switch in an extracellular loop, which may result from cleavage of the cytoplasmic amino and carboxy termini. In the centre of the water pathway, the closed pore in junctional AQP0 retains only three water molecules, which are too widely spaced to form hydrogen bonds with each other. Packing interactions between AQP0 tetramers in the crystalline array are mediated by lipid molecules, which assume preferred conformations. We were therefore able to build an atomic model for the lipid bilayer surrounding the AQP0 tetramers, and we describe lipid–protein interactions.

Members of the aquaporin (AQP) family form membrane pores that are either highly selective for water (aquaporins) or also permeable to other small neutral solutes such as glycerol and urea (aquaglyceroporins) (reviewed in ref. 1). Structural studies have revealed that all AQPs share the same basic architecture, which consists of two tandem repeats, each containing a bundle of three transmembrane α-helices and a hydrophobic loop with the highly conserved asparagine–proline–alanine (NPA) motif[2–8]. The two NPA-containing loops B and E fold back into the membrane and form short α-helices (HB and HE) that line the water pore. The ar/R constriction site, so named because it is formed by an aromatic residue and an arginine residue, confers water selectivity to AQP pores, whereas the NPA motifs are important in the proton exclusion mechanism (reviewed in ref. 9).

AQP0 is the most abundant protein in lens fibre cell membranes, where it forms not only water pores but also the 11–13-nm 'thin lens junctions' that assemble after proteolytic cleavage of the cytoplasmic termini[10,11]. We recently presented the structure of the AQP0-mediated membrane junction at 3 Å resolution as determined by electron crystallography of double-layered two-dimensional (2D) crystals[7]. The structure showed that AQP0 junctions are stabilized by specific interactions between tetramers in adjoining membranes involving proline residues almost exclusively. Calculated pore profiles also showed that the pore in junctional AQP0 is highly constricted by a substantially extended ar/R constriction site and a novel second constriction site[7], which may be involved in the pH regulation of AQP0 water conductance[12].

The 1.9 Å structure of junctional AQP0

The water pore in junctional AQP0 seen at 3 Å resolution appears closed[7]. However, the water molecules were not resolved and we were unable to demonstrate directly the absence of water molecules from the AQP0 pore. Using a better batch of 2D crystals (Fig. 1a), the carbon sandwich specimen preparation technique[13] and a helium-cooled top-entry 300-kV electron microscope[14], equipped with a field emission gun and a 4,096-pixel × 4,096-pixel charge-coupled device camera, we have now been able to collect electron diffraction data to much higher resolution.

Electron diffraction patterns collected from untilted specimens (Fig. 1b) as well as highly tilted specimens (Supplementary Fig. 1) showed strong and sharp diffraction spots to a resolution beyond 2 Å. The final data set comprised 286 diffraction patterns recorded at tilt angles of up to 71.3° that were merged to a resolution of 1.7 Å. The structure was refined with CNS[15] to a resolution of 1.9 Å using scattering factors for 300 kV electrons. The final refinement statistics are summarized in Table 1. At the improved resolution of 1.9 Å, water molecules can be identified clearly in the density map, and the rings of many aromatic residues are represented by doughnut-shaped densities (Fig. 1c).

Junctional versus non-junctional AQP0

The formation of thin junctions in the lens core correlates with proteolytic cleavage of at least a fraction of the AQP0 (refs 11, 16, 17). A comparison of the structure of AQP0 in the 2D crystals we describe here with that of AQP0 in three-dimensional (3D) crystals, as reported[8], allows us to identify differences between junctional and non-junctional conformations. In the 3D crystals, uncleaved AQP0 tetramers do not form junctions, and the pores are filled with water molecules[8]. In the double-layered 2D crystals, which form only from the partly proteolytically cleaved AQP0 population purified from lens core, the tetramers interact with each other through their extracellular surfaces (Supplementary Fig. 2b) and thus recapitulate the arrangment in the thin junctions between lens fibre cells[11]. In the junctional conformation the water pores are closed.

When we inspected the 3D crystal structure (Protein Data Bank accession code 1YMG) with PROCHECK[18] and WHATIF[19], we found that the unit-cell dimensions required adjustment (from $a = b = 110.53$ Å and $c = 53.39$ Å to $a = b = 109.53$ Å and $c = 52.82$ Å). We refined the structure into the adjusted cell and noticed continuous density for both termini (not built in the

[1]Department of Cell Biology and [2]Department of Biological Chemistry and Molecular Pharmacology, Harvard Medical School, 240 Longwood Avenue, Boston, Massachusetts 02115, USA. [3]Howard Hughes Medical Institute and Children's Hospital Laboratory of Molecular Medicine, 320 Longwood Avenue, Boston, Massachusetts 02115, USA. [4]Department of Biophysics, Kyoto University, Oiwake, Kitashirakawa Sakyo-ku, Kyoto 606-8502, Japan.

deposited model). We therefore modelled N-terminal residues 2–5 and C-terminal residues 240–263. The C terminus mediates important crystal packing contacts with two neighbouring tetramers (Supplementary Fig. 2a). Both termini also engage in interactions that seem to be of functional importance, as described in more detail below. The refinement (see Supplementary Table 1) improved the *G* factor[18] from −1.51 to 0.21.

In intact, non-junctional AQP0, the N-terminal and C-terminal regions have ordered conformations (Fig. 2b, c). Arg 226 and Lys 228 near the C terminus interact electrostatically with Ser 79, Gln 80 and Asp 150; the N terminus loops back and tucks Trp 2 into a hydrophobic pocket lined by Phe 9, Trp 10 and Leu 84 (Fig. 2c). The resulting conformation allows Glu 3 to interact with Ser 240, thereby bridging between the N-terminal and C-terminal segments. All these interactions are eliminated in truncated AQP0 (Fig. 2d, e). Cleavage at residue 234 causes the remainder of the C-terminal segment to move away from the membrane surface, disrupting the previous contacts of Arg 226 and Lys 228 (Fig. 2d). The N-terminal and C-terminal cleavages also eliminate Glu 3 and Ser 240.

How do these changes at the cytoplasmic face affect junctional interactions at the extracellular face? Disruption of the network of interactions involving the two termini seems to correlate with rearrangements in extracellular loop A (Fig. 2a). Pro 38 is particularly critical. In the non-junctional structure, this residue points away from the centre of the tetramer (Fig. 2f); moreover, Trp 34 lies above the pore and projects outward, blocking the approach of a second tetramer, and Arg 33 intervenes between two monomers. In the truncated, junctional AQP0 tetramer (Fig. 2g), loop A has reconfigured, positioning Pro 38 so that it can form a rosette-like structure at the centre of the tetramer and mediate a major junctional contact. Arg 33 and Trp 34 also swap positions, so that Trp 34 no longer interferes with the close approach of another tetramer. In the completed junction, all three residues interact with the corresponding residues from the apposing tetramer (the two Arg residues interact through a water molecule) (Supplementary Fig. 3).

Water molecules in the AQP0 pore

The water pore in non-junctional AQP0 contains seven water molecules (Fig. 3a, left); that in junctional AQP0 contains only three (Fig. 3a, right). The two pores have the same diameter over much of their lengths, but the pore in junctional AQP0 is narrower at the positions of the two constriction sites (Fig. 3a, centre). Constriction site I (CS-I) in non-junctional AQP0 spans 3 Å and has a minimum diameter of 2.31 Å; CS-I of junctional AQP0 extends over 10 Å and the pore narrows to 1.33 Å. The large difference in the length of CS-I is due mainly to the side chain of Met 176, which extends into the pore in junctional AQP0 (Supplementary Fig. 4a) but points away from it in non-junctional AQP0, allowing access by additional water molecules (Supplementary Fig. 4b). Constriction site II (CS-II) is narrower in junctional AQP0 (diameter 1.37 Å) than in non-junctional AQP0 (diameter 1.75 Å). The constricted pore in junctional AQP0 can thus accommodate only three water molecules, which seem to be trapped in the closed pore because it narrows above and below them (Supplementary Fig. 4c, d).

In our initial report of the closed water pore in junctional AQP0 (ref. 7), we proposed that AQP0 and other aquaporins might be in a dynamic equilibrium between an open and a closed pore conformation. We also suggested that pore closure might be triggered by the stabilization of an alternative conformation of Arg 187 (part of the ar/R constriction site) seen in the structure of junctional AQP0. A recent molecular dynamics study supports this notion: it showed that Arg 189 in AQPZ (corresponding to Arg 187 in AQP0) could adopt two conformations[20]. The 'UP' state, which is seen in most AQP crystal structures, had an open pore, filled by a continuous single file of water. The 'DOWN' state, seen in our structure of junctional AQP0, had a pore completely blocked by the Arg side chain, and prolonged blockage resulted in the loss of all water molecules from the pore. Although attractive, a conformational switch of the arginine in the ar/R constriction site cannot be the only mechanism for AQP gating, because Arg 187 is in the 'DOWN' state not only in our closed, junctional AQP0 but also in the open, non-junctional AQP0 structure[8]. The main difference between the open pore and the closed pore lies in the conformation of the side chain of Met 176 (see above), a residue not present in AQPZ.

The distances between the three water molecules (4 Å or more) in the closed pore are too long for hydrogen bonding (Fig. 3b, right, and Supplementary Fig. 5, right). The water coordinated to the Asn residues of the two NPA motifs donates a hydrogen bond to the hydroxyl group of Tyr 24, which in turn donates a hydrogen bond to the water molecule in the extracellular half of the water pathway (Fig. 3b, right, and Supplementary Fig. 5, right). The corresponding two water molecules in the open water pore of non-junctional AQP0 have the same hydrogen-bonding pattern (Fig. 3b, left, and Supplementary Fig. 5, left), and all the other water molecules are within

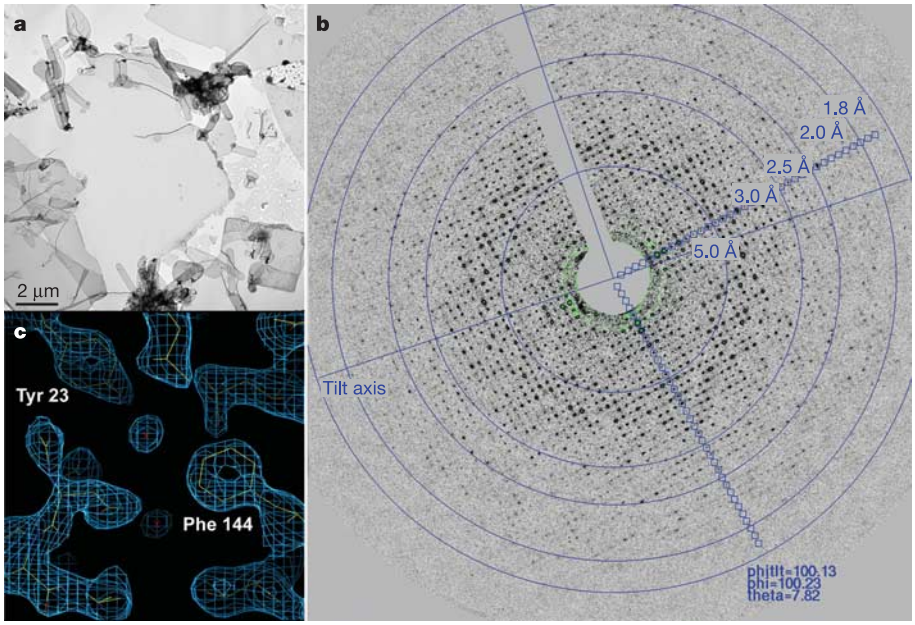

Figure 1 | Electron crystallography of AQP0 junctions. a, Double-layered AQP0 2D crystals were often several micrometres in size. **b**, A typical electron diffraction pattern recorded from an untilted AQP0 2D crystal prepared by the carbon sandwich technique[13], showing diffraction spots to a resolution beyond 2 Å. **c**, Region of the final $2F_o - F_c$ map of AQP0 refined to 1.9 Å resolution. Two aromatic residues, Tyr 23 and Phe 144, that line the water pore in AQP0 are represented by doughnut-shaped densities.

Table 1 | Electron crystallographic data

Two-dimensional crystals	
Layer group	*p*422
Unit cell (Å)	$a = b = 65.5$
Thickness (assumed) (Å)	160
Electron diffraction	
Number of patterns merged	286 (0°, 11; 20°, 43; 45°, 107; 60°, 87; 70°, 38)
Resolution limit for merging (Å)	1.7
$R_{Friedel}$ (%)	14.25
R_{merge} (%)	16.60
Observed amplitudes to 1.9 Å	126,980
Unique reflections	22,293
Maximum tilt angle (°)	71.3
Fourier space sampled	80.0% (70.5% at 2.0–1.9 Å)
Multiplicity	5.7 (2.5 at 2.0–1.9 Å)
Crystallographic refinement (5.0–1.9 Å)	
Resolution limit for refinement (Å)	1.9
Crystallographic *R* factor (%)	25.81
Free *R* factor (%)	29.93
Reflections in working/test set	14,600/1,580
Non-hydrogen protein atoms	1,784
Non-hydrogen lipid atoms	348
Solvent molecules	76
Average protein *B* factor (Å^2)	48.4
Ramachandran plot (%)	97.5; 2.5; 0 (allowed; generous; disallowed)

R_{free} is calculated from a randomly chosen 10% of reflections, and R_{cryst} is calculated over the remaining 90% of reflections.

hydrogen-bonding distance of each other. This 'phenolic barrier' created by Tyr 24, a residue not seen in the other known AQP structures, may be responsible for the poor water conductance of AQP0 in comparison with other AQPs, which contain a continuous line of hydrogen-bonded water molecules. The space occupied by Tyr 24 might also explain why the open AQP0 pore contains only seven water molecules, whereas molecular dynamics studies showed eight water molecules in AQP1 (refs 21, 22) and AQPZ[20] and nine in GlpF[23].

AQP0 water conductance is dependent on pH, with a maximum at pH 6.5 and only about half the activity at pH 10.5 (ref. 12). These conductance characteristics are not changed by proteolytic cleavage of AQP0 (ref. 24). As our structure, obtained with the double-layered 2D crystals grown at pH 6 (ref. 7), reveals fewer water molecules in the pore than the structure determined from the 3D crystals grown at pH 10.5 (ref. 8), pore closure seems to be a result of junction formation, not pH shift.

Lipid–protein interactions

Crystals of membrane proteins occasionally contain lipid molecules. For example, the structure of bacteriorhodopsin from lipid cubic-phase crystallization revealed 13 phytanyl lipids, 7 of which formed a bilayer structure, and a squalene[25]. These, and all other lipids found in crystal structures so far (78 lipids in total[26]), originate from the native membrane, from which they co-purify with the crystallized membrane protein. Such tightly bound lipids have been found to be essential for the structural integrity and activity of a number of membrane proteins[27].

None of the AQP 3D crystals examined so far contain lipids, and 2D crystals of AQPs can form with a variety of different lipids, indicating that AQPs might have neither a requirement for specific lipids nor high-affinity lipid-binding sites. Nevertheless, our density map revealed that between the AQP0 tetramers are horseshoe-shaped features characteristic of lipid molecules (Fig. 4a). Indeed, close inspection revealed that lipids bridge all the contacts between tetramers within a layer and that the tetramers have essentially no direct lateral interaction. In composite omit maps we could identify nine lipids per AQP0 monomer, which we modelled as complete or

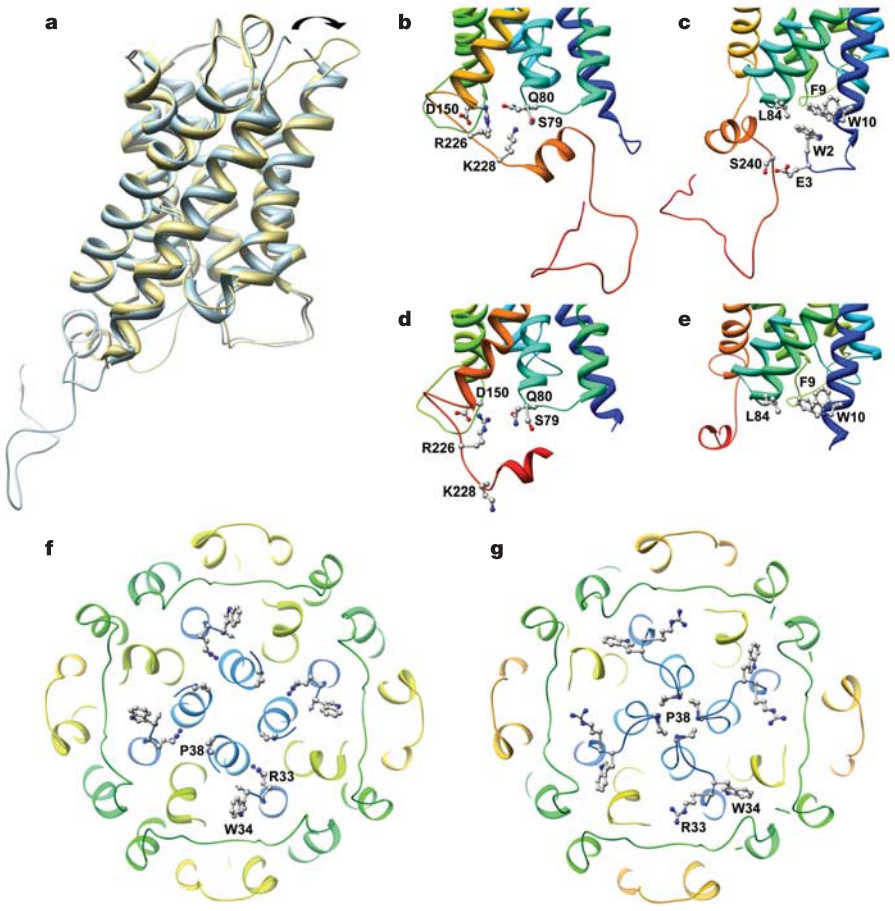

Figure 2 | Structural differences between junctional and non-junctional AQP0. a, X-ray structure of non-junctional AQP0 (blue) superimposed on the electron-microscope structure of junctional AQP0 (yellow). The arrow indicates the conformational switch of extracellular loop A. **b**, Interactions involving the C terminus of full-length AQP0. **c**, Interactions involving the N terminus of full-length AQP0. **d**, C terminus of cleaved AQP0. **e**, N terminus of cleaved AQP0. **f**, View of the extracellular surface of the X-ray structure of non-junctional, full-length AQP0. **g**, View of the extracellular surface of the electron-microscope structure of junctional AQP0 from the lens core, showing the rosette-like structure formed by the Pro 38 residues.

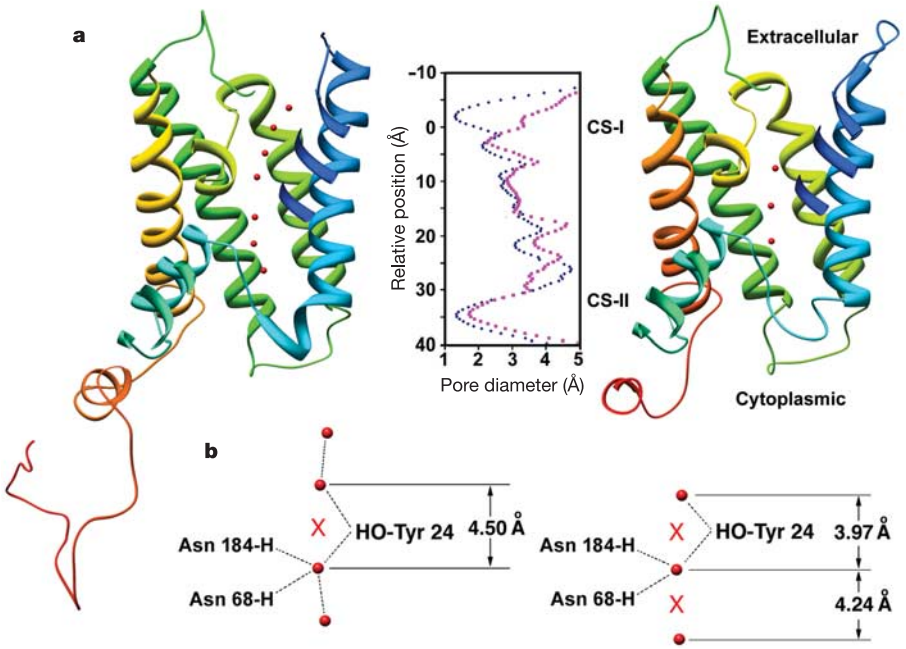

Figure 3 | **The water pore in AQP0.** **a**, The pore in non-junctional AQP0 (left) contains seven water molecules (red spheres), whereas the pore in junctional AQP0 contains only three water molecules (right). Calculated pore profiles (middle) confirm that the pore in junctional AQP0 (purple) is more constricted than that in non-junctional AQP0 (pink). **b**, Hydrogen-bonding pattern of water molecules in the pore of non-junctional AQP0 (left) and junctional AQP0 (right). The hydrogen-bonding network is disrupted by Tyr 24, which introduces a phenolic barrier. In junctional AQP0 all three water molecules are too far apart to form hydrogen bonds. Dotted lines represent hydrogen bonds. See Supplementary Fig. 5.

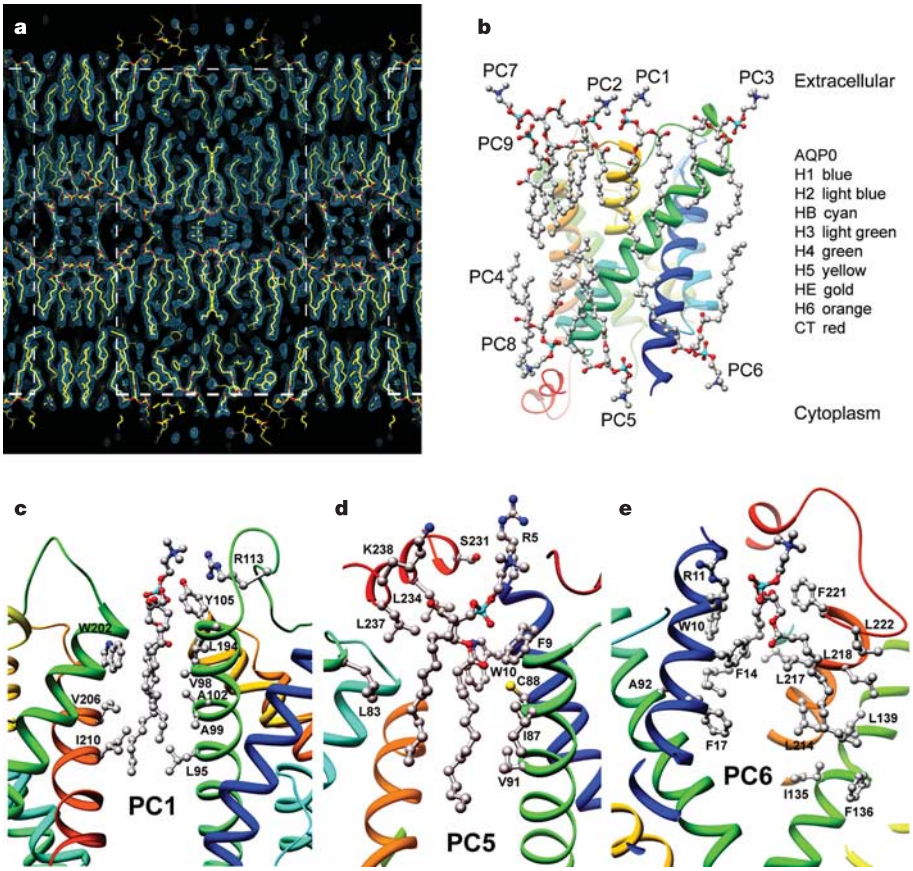

Figure 4 | **Lipid–protein interactions in double-layered AQP0 2D crystals.** **a**, Vertical slab through the $2F_o - F_c$ density map with modelled lipid molecules, revealing the two lipid bilayers in the double-layered AQP0 2D crystal. **b**, The nine lipids surrounding an AQP0 monomer in the 2D crystal. Lipids PC1 to PC7 are annular lipids, whereas lipids PC8 and PC9 are bulk lipids with no direct protein contacts. H1–H6, helices 1–6; CT, cytoplasmic tail. See Supplementary Fig. 6 for a stereo view. **c**–**e**, Three examples of lipids sandwiched between two AQP0 molecules. The acyl chains of PC1 adopt a closed conformation (**c**), those of PC5 a slightly splayed conformation (**d**) and those of PC6 a widely splayed conformation (**e**).

partial molecules of dimyristoyl phosphatidyl choline (DMPC, the lipid used for 2D crystallization) (Fig. 4a). Phospholipid headgroups have a chiral centre at C2 of the glycerol, and the DMPC we used is a racemic mixture. Density is weak or absent at most C2 positions in our map, and often at the attached ester group as well, indicating that there might be little or no selectivity for the biological enantiomer. Very strong density for the phosphate groups, weaker but well-defined density for the trimethylamine groups of the cholines, and unambiguous density for the acyl chains allowed us to build and refine a model in which we chose an enantiomer for each lipid more or less arbitrarily. We have not yet attempted to refine the two alternatives with 50% occupancy each. We have annotated these lipids as PC1 to PC9 (Fig. 4b and Supplementary Fig. 6). PC1 to PC7 have extensive protein contacts and seem to represent 'annular lipids' immediately adjacent to a membrane-embedded protein. PC8 and PC9 are not in contact with protein and thus represent bulk lipids. A detailed description of lipid–protein contacts is provided in Supplementary Materials. As AQP0 has no tight lipid-binding sites, interactions between the annular lipids and the AQP0 subunits are likely to represent the kinds of contact that occur between any membrane protein and the lipids surrounding it.

Annular lipids must adapt to the irregular surface of a transmembrane protein to create a smooth interface for bulk lipids. This fit limits the mobility (and perhaps the chemistry) of annular lipids, because their conformations are partly defined by the protein surface. In our 2D arrays, most of the annular lipids are sandwiched between two tetramers and thus mediate lattice interactions (Supplementary Fig. 7). This packing further restricts their conformations. The cell dimensions of our reconstituted junctions are the same as those in thin junctions between lens fibre cells[28]. We therefore suggest that the lipid–protein interactions we observe in our 2D crystals with the artificial lipid DMPC are representative of those formed by AQP0 tetramers with native lipids in lens fibre cell membranes.

The lipids form a one-molecule-wide annular shell around the protein. The positions of the headgroups vary by only ± 2 Å in the direction perpendicular to the membrane plane, with a separation of about 34 Å from phosphate to phosphate. The dimensions of the bilayer correspond closely to those of fully hydrated, fluid-phase DMPC[29]. A hydrated network of hydrogen bonds and salt bridges holds the lipid phosphates in place. Protein groups interacting with phosphates include three arginine side chains, a tyrosine hydroxyl group that mediates one of the arginine contacts, a lysine, a tryptophan indole nitrogen, a glutamine side-chain amide, and at least one main-chain amide. Similar interactions have been described for specifically bound lipids[30].

Acyl chains fill the gaps between adjacent tetramers. Their conformations clearly adapt to the knobs and grooves of the apposed hydrophobic protein surfaces. Figure 4c–e illustrates three examples. PC1 in the extracellular leaflet is the best ordered of the nine DMPC molecules. Its acyl chains are nearly fully extended, packed against those of PC2 and PC3 and sandwiched between five nonpolar side chains from one AQP0 molecule and three from the other. PC5 in the cytoplasmic leaflet has somewhat less extended acyl chains. The phosphate receives a hydrogen bond from the indole nitrogen of Trp 10 and Lys 238 (as well as the poorly ordered N-terminal segment) of an adjacent subunit. The acyl chains, packed between those of PC4 and PC6, contact four hydrophobic side chains from one subunit (including the hydrophobic face of Trp 10) and three from another. PC6, also in the cytoplasmic leaflet, has widely splayed acyl chains, separated by side chains from the two apposed AQP0 molecules. Phe 14 of one molecule and Leu 217 of another are in van der Waals contact through the gap: this is the only direct interaction between tetramers within a layer.

PC8 and PC9 lie near the four-fold axis. They do not contact protein and thus represent bulk lipids. Neither is as well ordered as the annular lipids. Indeed, PC8 (in the cytoplasmic leaflet) is probably only statistically ordered (two, rather than four, molecules about a four-fold axis), because there is space for only one of the two acyl chains and no density for the headgroup. The headgroup of PC9 lies about 3 Å closer to the midplane of the bilayer than those of the four other extracellular leaflet lipids; the bilayer thickness may therefore be influenced by adjacency to the protein.

Discussion

AQP0 serves a dual function in the lens, acting both as a water channel and as an adhesion molecule. During the differentiation of fibre cells, and as they grow older and become buried more deeply in the lens, AQP0 is cleaved at both termini[16,17,31,32]. This processing seems to be the trigger for junction formation[10,11]. Comparison of our structure of junctional AQP0 with that of non-junctional AQP0 (ref. 8) indicates that cleavage of the two cytoplasmic termini might translate into a conformational switch in extracellular loop A, eliminating steric hindrance from Trp 34 and allowing Pro 38 to stabilize the junctional interaction. Formation of the junction also seems to correlate with changes in the side-chain positions of residues lining the pore, most importantly in Met 176, resulting in substantial constriction. Three water molecules are trapped in the centre of the water pathway, too far apart from each other to be linked by hydrogen bonds.

Mutations in AQP0 result in cataracts[33–37]. Most of these mutations interfere with the correct trafficking of AQP0 to the plasma membrane (reviewed in ref. 38), rather than with efficient water conduction as proposed recently[8]. However, the mutations might prevent proper interaction with lipid, which in many instances has a key role in the folding and integration of membrane proteins into a bilayer[30,39,40].

The lipids in our 2D crystals indeed demonstrate a well-defined role for annular lipids in forming a boundary for the bilayer-inserted protein. The headgroup interactions of these lipids resemble those described for specifically bound lipids[30], and the acyl chains are tightly packed around the laterally projecting hydrophobic side chains of the protein. We suggest that when junctions form between lens fibre cells, the annular lipids already partly immobilized by interaction with AQP0 mediate the lattice contacts, just as DMPC does in our reconstituted junctions. Although the composition of natural membrane lipids is far less homogeneous than in our crystals, the incorporation of both DMPC enantiomers shows that the headgroup interactions are somewhat adjustable, and imperfect crystallinity of the acyl chains indicates that C_{16} or C_{18} chains, or even unsaturated chains, could readily be accommodated. It remains to be determined whether AQP0 exhibits selectivity for its annular lipids and hence for the lipid composition within the junctional lattices.

METHODS

Purification and 2D crystallization of AQP0 from the lens core. AQP0 was purified from the core of sheep lenses and reconstituted into 2D crystals as described previously[7]. The 2D crystals were grown at a lipid:protein ratio of 0.25 (by mass), which corresponds to a molar ratio of 37 lipids per AQP0 tetramer. This is very close to the number of lipids, 36, that we could model per AQP0 tetramer.

Electron microscopy and data processing. Negatively stained samples were prepared and imaged as described previously[7]. Specimens for cryoelectron microscopy were prepared as described[13]. In brief, double-layered AQP0 2D crystals were mixed with an equal amount of 10% trehalose and the suspension was applied to a molybdenum grid covered with a thin carbon film. The grid was blotted to remove excess material, and a second carbon film was placed on top of the sample. Grids were plunged into liquid nitrogen and loaded into a JEM3000SFF electron microscope equipped with a top-entry helium stage and operated at an acceleration voltage of 300 kV (ref. 14). Low-dose electron diffraction patterns were recorded with a 4,096-pixel × 4,096-pixel charge-coupled-device camera (Gatan). Electron diffraction patterns were analysed and merged as described[41].

Molecular replacement, model building and refinement. The structure of AQP0 was determined by molecular replacement as described previously[7]. Crowther fast cross-rotation function calculations identified an orientation of a single subunit in the asymmetric unit as the top solution with a rotation

function signal double the value of the second peak. The translation function gave a top solution with an R factor of 42.7% and a correlation coefficient of 84.3%. The model was refined with CNS version 1.1 (ref. 15). Rigid-body refinement was used to evaluate what scattering factors to use. In a resolution range of 10–2.5 Å, both X-ray and electron scattering factors for 120-kV electrons[41] produced comparable results. In a resolution range of 10–1.9 Å, electron scattering factors for 300-kV electrons produced the best result ($R = 35.92\%$), in comparison with electron scattering factors for 120-kV electrons ($R = 67.06\%$) and X-ray scattering factors ($R = 37.39\%$). For all subsequent refinement steps, refinement was performed in a resolution range of 5–1.9 Å without bulk solvent flattening, using a unit cell of $a = b = 65.5$ Å, an assumed thickness of 160 Å, and electron scattering factors for 300-kV electrons. Model building was performed with O[42] using $2F_o - F_c$ density maps and simulated annealing composite omit maps. Protein residues 5–239 were visible and were modelled (major cleavage sites *in vivo*[32]), together with nine lipid (DMPC) and 76 water molecules. The model was refined by cycles of simulated annealing, *B*-factor refinement, and remodelling. The final refinement statistics are presented in Table 1.

For the crystal structure of non-junctional AQP0 (ref. 8) we downloaded the structure factors and coordinates from the Protein Data Bank (accession code 1YMG). The structure was evaluated with PROCHECK[18] and WHATIF[19] and the unit cell dimensions were adjusted from $a = b = 110.531$ Å and $c = 53.390$ Å to $a = b = 109.531$ Å and $c = 52.822$ Å. A composite omit map was calculated and a clear continuous density was observed for both the N terminus and the C terminus. We modelled N-terminal residues 2–5 and C-terminal residues 240–263 in O[42] and refined the structure in CNS version 1.1 (ref. 15) by cycles of simulated annealing, *B*-factor refinement, and remodelling. The final refinement statistics are presented in Supplementary Table 1.

Received 6 September; accepted 12 October 2005.

1. Agre, P. *et al.* Aquaporin water channels—from atomic structure to clinical medicine. *J. Physiol. (Lond.)* **542,** 3–16 (2002).
2. Murata, K. *et al.* Structural determinants of water permeation through aquaporin-1. *Nature* **407,** 599–605 (2000).
3. Fu, D. *et al.* Structure of a glycerol-conducting channel and the basis for its selectivity. *Science* **290,** 481–486 (2000).
4. Sui, H., Han, B. G., Lee, J. K., Walian, P. & Jap, B. K. Structural basis of water-specific transport through the AQP1 water channel. *Nature* **414,** 872–878 (2001).
5. Ren, G., Reddy, V. S., Cheng, A., Melnyk, P. & Mitra, A. K. Visualization of a water-selective pore by electron crystallography in vitreous ice. *Proc. Natl Acad. Sci. USA* **98,** 1398–1403 (2001).
6. Savage, D. F., Egea, P. F., Robles-Colmenares, Y., O'Connell, J. D. & Stroud, R. M. Architecture and selectivity in aquaporins: 2.5 Å X-ray structure of aquaporin Z. *PLoS Biol.* **1,** E72 (2003).
7. Gonen, T., Sliz, P., Kistler, J., Cheng, Y. & Walz, T. Aquaporin-0 membrane junctions reveal the structure of a closed water pore. *Nature* **429,** 193–197 (2004).
8. Harries, W. E., Akhavan, D., Miercke, L. J., Khademi, S. & Stroud, R. M. The channel architecture of aquaporin 0 at a 2.2-Å resolution. *Proc. Natl Acad. Sci. USA* **101,** 14045–14050 (2004).
9. de Groot, B. L. & Grubmuller, H. The dynamics and energetics of water permeation and proton exclusion in aquaporins. *Curr. Opin. Struct. Biol.* **15,** 176–183 (2005).
10. Kistler, J. & Bullivant, S. Lens gap junctions and orthogonal arrays are unrelated. *FEBS Lett.* **111,** 73–78 (1980).
11. Gonen, T., Cheng, Y., Kistler, J. & Walz, T. Aquaporin-0 membrane junctions form upon proteolytic cleavage. *J. Mol. Biol.* **342,** 1337–1345 (2004).
12. Nemeth-Cahalan, K. L., Kalman, K. & Hall, J. E. Molecular basis of pH and Ca^{2+} regulation of aquaporin water permeability. *J. Gen. Physiol.* **123,** 573–580 (2004).
13. Gyobu, N. *et al.* Improved specimen preparation for cryo-electron microscopy using a symmetric carbon sandwich technique. *J. Struct. Biol.* **146,** 325–333 (2004).
14. Fujiyoshi, Y. The structural study of membrane proteins by electron crystallography. *Adv. Biophys.* **35,** 25–80 (1998).
15. Brunger, A. T. *et al.* Crystallography & NMR system: a new software suite for macromolecular structure determination. *Acta Crystallogr. D Biol. Crystallogr.* **54,** 905–921 (1998).
16. Roy, D., Spector, A. & Farnsworth, P. N. Human lens membrane: comparison of major intrinsic polypeptides from young and old lenses isolated by a new methodology. *Exp. Eye Res.* **28,** 353–358 (1979).
17. Takemoto, L., Takehana, M. & Horwitz, J. Covalent changes in MIP26K during aging of the human lens membrane. *Invest. Ophthalmol. Vis. Sci.* **27,** 443–446 (1986).
18. Laskowski, R. A., MacArthur, M. W., Moss, D. S. & Thornton, J. M. PROCHECK: a program to check the stereochemical qaulity of protein structures. *J. Appl. Crystallogr.* **26,** 283–291 (1993).
19. Vriend, G. WHAT IF: a molecular modeling and drug design program. *J. Mol. Graph.* **8,** 526–529 (1990).
20. Wang, Y., Schulten, K. & Tajkhorshid, E. What makes an aquaporin a glycerol channel? A comparative study of AqpZ and GlpF. *Structure* **13,** 1107–1118 (2005).
21. de Groot, B. L. & Grubmuller, H. Water permeation across biological membranes: mechanism and dynamics of aquaporin-1 and GlpF. *Science* **294,** 2353–2357 (2001).
22. Zhu, F., Tajkhorshid, E. & Schulten, K. Molecular dynamics study of aquaporin-1 water channel in a lipid bilayer. *FEBS Lett.* **504,** 212–218 (2001).
23. Tajkhorshid, E. *et al.* Control of the selectivity of the aquaporin water channel family by global orientational tuning. *Science* **296,** 525–530 (2002).
24. Ball, L. E. *et al.* Water permeability of C-terminally truncated aquaporin 0 (AQP0 1–243) observed in the aging human lens. *Invest. Ophthalmol. Vis. Sci.* **44,** 4820–4828 (2003).
25. Luecke, H., Schobert, B., Richter, H. T., Cartailler, J. P. & Lanyi, J. K. Structure of bacteriorhodopsin at 1.55 Å resolution. *J. Mol. Biol.* **291,** 899–911 (1999).
26. Wiener, M. in *Protein–Lipid Interactions: From Membrane Domains to Cellular Networks* (ed. Tamm, L. K.) 29–49 (Wiley-VCH, Weinheim, 2005).
27. Dowhan, W. Molecular basis for membrane phospholipid diversity: why are there so many lipids? *Annu. Rev. Biochem.* **66,** 199–232 (1997).
28. Zampighi, G., Simon, S. A., Robertson, J. D., McIntosh, T. J. & Costello, M. J. On the structural organization of isolated bovine lens fiber junctions. *J. Cell Biol.* **93,** 175–189 (1982).
29. Kucerka, N. *et al.* Structure of fully hydrated fluid phase DMPC and DLPC lipid bilayers using X-ray scattering from oriented multilamellar arrays and from unilamellar vesicles. *Biophys. J.* **88,** 2626–2637 (2005).
30. Palsdottir, H. & Hunte, C. Lipids in membrane protein structures. *Biochim. Biophys. Acta* **1666,** 2–18 (2004).
31. Schey, K. L., Little, M., Fowler, J. G. & Crouch, R. K. Characterization of human lens major intrinsic protein structure. *Invest. Ophthalmol. Vis. Sci.* **41,** 175–182 (2000).
32. Ball, L. E., Garland, D. L., Crouch, R. K. & Schey, K. L. Post-translational modifications of aquaporin 0 (AQP0) in the normal human lens: spatial and temporal occurrence. *Biochemistry* **43,** 9856–9865 (2004).
33. Shiels, A. & Bassnett, S. Mutations in the founder of the *MIP* gene family underlie cataract development in the mouse. *Nature Genet.* **12,** 212–215 (1996).
34. Shiels, A., Mackay, D., Bassnett, S., Al-Ghoul, K. & Kuszak, J. Disruption of lens fiber cell architecture in mice expressing a chimeric AQP0-LTR protein. *FASEB J.* **14,** 2207–2212 (2000).
35. Francis, P. *et al.* Functional impairment of lens aquaporin in two families with dominantly inherited cataracts. *Hum. Mol. Genet.* **9,** 2329–2334 (2000).
36. Francis, P., Berry, V., Bhattacharya, S. & Moore, A. Congenital progressive polymorphic cataract caused by a mutation in the major intrinsic protein of the lens, MIP (AQP0). *Br. J. Ophthalmol.* **84,** 1376–1379 (2000).
37. Okamura, T. *et al.* Bilateral congenital cataracts result from a gain-of-function mutation in the gene for aquaporin-0 in mice. *Genomics* **81,** 361–368 (2003).
38. Chepelinsky, A. B. The ocular lens fiber membrane specific protein MIP/aquaporin 0. *J. Exp. Zool. A* **300,** 41–46 (2003).
39. Lee, A. G. How lipids affect the activities of integral membrane proteins. *Biochim. Biophys. Acta* **1666,** 62–87 (2004).
40. Jensen, M. O. & Mouritsen, O. G. Lipids do influence protein function—the hydrophobic matching hypothesis revisited. *Biochim. Biophys. Acta* **1666,** 205–226 (2004).
41. Mitsuoka, K. *et al.* The structure of bacteriorhodopsin at 3.0 Å resolution based on electron crystallography: implication of the charge distribution. *J. Mol. Biol.* **286,** 861–882 (1999).
42. Jones, T. A., Zou, J. Y., Cowan, S. W. & Kjeldgaard, M. Improved methods for building protein models in electron density maps and the location of errors in these models. *Acta Crystallogr. A* **47,** 110–119 (1991).

Supplementary Information is linked to the online version of the paper at www.nature.com/nature.

Acknowledgements This work was supported by NIH funding (to T.W.) and a Grant-in Aid for Specially Promoted Research (to Y.F.).

Author Information Coordinates and structure factors for junctional and non-junctional AQP0 have been deposited in the Protein Data Bank (accession codes 2B6O and 2B6P, respectively). Reprints and permissions information is available at npg.nature.com/reprintsandpermissions. The authors declare no competing financial interests. Correspondence and requests for materials should be addressed to T.W. (twalz@hms.harvard.edu).